# Analytic theory of an edge mode between impedance surfaces

Xianghong Kong,[1,2,*] Dia'aaldin J. Bisharat,[2,†] Gaobiao Xiao,[1,‡] and Daniel F. Sievenpiper[2,§]
[1]*Department of Electronic Engineering, Shanghai Jiao Tong University, Shanghai 200240, China*
[2]*Electrical and Computer Engineering Department, University of California, San Diego, California 92093, USA*

(Received 25 October 2018; published 21 March 2019)

An eigenmode analysis is presented of the electromagnetic field which occurs between two complementary surface impedances. The analysis is based on the generalized reflection method which is a generalization of the Sommerfeld-Maliuzhinets technique. Numerical results are presented and validated against independent COMSOL simulations. Also, the characteristic impedance and phase velocity are defined and calculated for further investigation of the structure.

DOI: 10.1103/PhysRevA.99.033842

## I. INTRODUCTION

Edge modes can be widely found in quantum phenomena [1,2], optics [3–6], and acoustics [7,8]. Because of the complexity of such structures, it is almost impossible to obtain the exact closed-form solutions of the edge modes. However, a simple structure has been discovered which confines the energy along the interface between two planar surfaces recently [9–11]. It has been shown that the line wave occurs when the surface impedances on the two sides are complementary, which means one is inductive while the other is capacitive. Both numerical simulation and experimental verification have demonstrated these line waves, but an analytical solution has only been found for the limiting case where the two surfaces are perfect electric and perfect magnetic conductors.

In this paper, we apply the generalized reflection method to the eigenmode solution of a wedge with two different impedance boundary conditions. The generalized reflection method is developed by Vaccaro to study the scattering from an impedance wedge excited by an obliquely incident plane wave as shown in Fig. 1(a) [12,13]. The generalized reflection method is the generalization of the Sommerfeld-Maliuzhinets method, which is applied to solve the problem of the scattering wave of a wedge with impedance surfaces excited by a normally incident plane wave [14]. The TM and TE polarized wave are coupled for the oblique incidence, which makes the Maliuzhinets method no longer valid. Based on the Sommerfeld-Maliuzhinets technique, the diffraction of an electromagnetic skew-incident wave by a wedge with anisotropic impedance boundary condition is solved analytically [15,16]. The scattered wave generated by a Hertzian dipole placed over an impedance wedge can be calculated by expanding the dipole field into plane waves and extending to complex angles of incidence [17].

However, to the best of the authors' knowledge, no satisfactory analytic solution to the eigenmode on an impedance wedge exists. Knowing the eigenmode solution not only helps us to understand the driven mode such as the scattered wave of a wedge excited by plane wave or dipole, but also gives a deeper understanding on the edge mode between impedance surfaces.

## II. THEORETICAL ANALYSIS

### A. Structure description

Similar to the driven mode analysis, we have two semi-infinite surfaces with complementary surface impedances $Z_1$ and $Z_2$ as shown in Fig. 1(b), which means $\mathrm{Im}(Z_1)\mathrm{Im}(Z_2) < 0$. However, instead of solving for scattering by an incident wave, we find the eigenmode solution. For simplicity, we assume the surface is lossless, so $\mathrm{Re}(Z_1) = \mathrm{Re}(Z_2) = 0$. We also assume the angle between two surfaces is $\pi$, which is the same as in Ref. [9]. All the fields in the following discussion have the $e^{-i\omega t}$ time dependence, which is suppressed. The surfaces of the wedge satisfy the Leontovich boundary condition [18]:

$$\vec{E} - \hat{\phi}(\hat{\phi}\cdot\vec{E}) = \hat{\phi}\times\vec{H}Z_1, \tag{1a}$$

$$\vec{E} - \hat{\phi}(\hat{\phi}\cdot\vec{E}) = -\hat{\phi}\times\vec{H}Z_2, \tag{1b}$$

where $\hat{\phi}$ is the unit vector as shown in Fig. 1(a).

### B. Generalized reflection method

By applying the Sommerfeld-Maliuzhinets technique, we can transform the electromagnetic field from real space to the spectral domain:

$$\bar{f}_z(\rho,\phi,z) = \frac{e^{ik_0 z\cos\beta}}{2\pi i}\int_\gamma \bar{F}_z\Big(\alpha+\frac{\pi}{2}-\phi\Big)e^{-ik_0\rho\sin\beta\cos\alpha}d\alpha, \tag{2}$$

where $\bar{f}_z(\rho,\phi,z) = \left[\begin{smallmatrix}E_z\\ Z_0H_z\end{smallmatrix}\right]$ and $Z_0$ is the free space intrinsic impedance. The column vector $\bar{F}_z(\alpha)$ represents the spectral function for $E_z$ and $Z_0H_z$. For the driven mode, $\beta$ is the angle between the incident wave and the $\hat{z}$ axis, which is a

*klovek@sjtu.edu.cn
†dbisharat@eng.ucsd.edu
‡gaobiaoxiao@sjtu.edu.cn
§dsievenpiper@eng.ucsd.edu

 

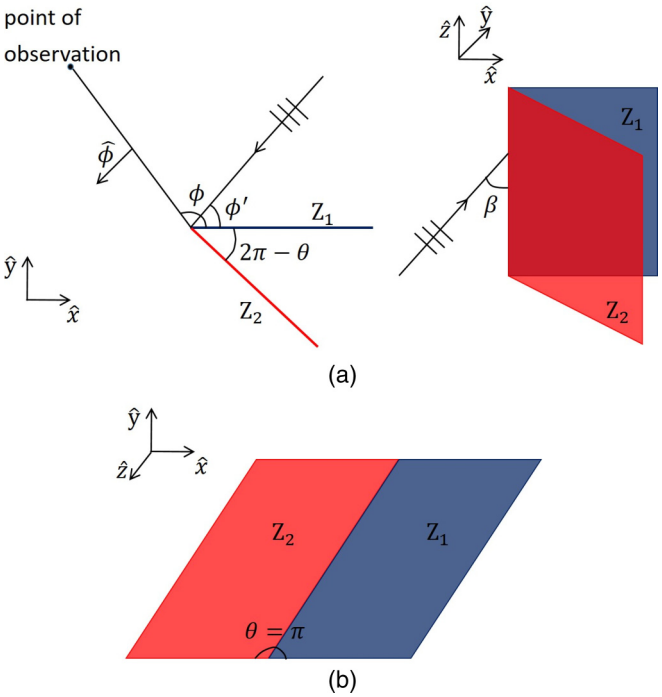


FIG. 1. (a) Impedance wedge with obliquely incident plane wave. The angle between impedance faces is $\theta$. (b) Line wave structure shown in Ref. [9] when $\theta=\pi$.

given parameter. However, for the eigenmode case, $\beta$ is the eigenvalue that we need to find by solving Maxwell equations. It is proven that for the wedge structure the $z$ components of the electric and magnetic fields are bounded at the edge, $|E_z(\rho=0)|<\infty$ and $|H_z(\rho=0)|<\infty$, while $|E_\rho|$, $|E_\phi|$, $|H_\rho|$, and $|H_\phi|$ will tend to infinity [19]. The behavior of $\bar{f}_z(\rho,\phi,z)$ at $\rho\to 0$ is related to the behavior of the spectral function $\bar{F}_z(\alpha)$ at $|\mathrm{Im}(\alpha)|\to\infty$:

$$\lim_{|\mathrm{Im}(\alpha)|\to\infty}\bar{F}_z(\alpha)=\text{constant}. \tag{3}$$

Applying the impedance boundary condition as shown in Eqs. (1a) and (1b) to the spectral expression Eq. (2), we can get [18]

$$\begin{aligned}&(\bar{\bar{I}}\sin\alpha+\sin\bar{\bar{v}}_1)\bar{\bar{C}}(\alpha)\bar{F}_z\Big(\alpha+\frac{\pi}{2}\Big)\\&\quad=(-\bar{\bar{I}}\sin\alpha+\sin\bar{\bar{v}}_1)\bar{\bar{C}}(-\alpha)\bar{F}_z\Big(-\alpha+\frac{\pi}{2}\Big),\end{aligned} \tag{4a}$$

$$\begin{aligned}&(\bar{\bar{I}}\sin\alpha-\sin\bar{\bar{v}}_2)\bar{\bar{C}}(\alpha)\bar{F}_z\Big(\alpha-\frac{\pi}{2}\Big)\\&\quad=(-\bar{\bar{I}}\sin\alpha-\sin\bar{\bar{v}}_2)\bar{\bar{C}}(-\alpha)\bar{F}_z\Big(-\alpha-\frac{\pi}{2}\Big),\end{aligned} \tag{4b}$$

where

$$\bar{\bar{C}}(\alpha)=\begin{bmatrix}\cos\alpha & -\sin\alpha\cos\beta\\ \sin\alpha\cos\beta & \cos\alpha\end{bmatrix}, \tag{5}$$

$$\sin\bar{\bar{v}}_{1,2}=\begin{bmatrix}\sin v^e_{1,2} & 0\\ 0 & \sin v^h_{1,2}\end{bmatrix}=\begin{bmatrix}\frac{Y_{1,2}}{Y_0\sin\beta} & 0\\ 0 & \frac{Z_{1,2}}{Z_0\sin\beta}\end{bmatrix}, \tag{6}$$

and $\bar{\bar{I}}$ is the $2\times 2$ identity matrix. $Y_0=1/Z_0$ is the free-space admittance and $Y_{1,2}=1/Z_{1,2}$.

As shown in Eqs. (4a) and (4b), the two components in $\bar{F}_z(\alpha)$ are coupled since the matrix $\bar{\bar{C}}(\alpha)$ is nondiagonal. In order to solve $\bar{F}_z(\alpha)$ efficiently, we rewrite Eqs. (4a) and (4b) by variable substitution:

$$\bar{F}_z(\alpha)=\bar{\bar{C}}^{-1}\Big(\alpha-\frac{\pi}{2}\Big)\bar{G}_z(\alpha). \tag{7}$$

Then we have

$$\begin{aligned}&(\bar{\bar{I}}\sin\alpha+\sin\bar{\bar{v}}_1)\bar{G}_z\Big(\alpha+\frac{\pi}{2}\Big)\\&\quad=(-\bar{\bar{I}}\sin\alpha+\sin\bar{\bar{v}}_1)\bar{G}_z\Big(-\alpha+\frac{\pi}{2}\Big),\end{aligned} \tag{8a}$$

$$\begin{aligned}&(\bar{\bar{I}}\sin\alpha-\sin\bar{\bar{v}}_2)\bar{G}_z\Big(\alpha-\frac{\pi}{2}\Big)\\&\quad=(-\bar{\bar{I}}\sin\alpha-\sin\bar{\bar{v}}_2)\bar{G}_z\Big(-\alpha-\frac{\pi}{2}\Big).\end{aligned} \tag{8b}$$

For Eqs. (8a) and (8b), the two components of $\bar{G}_z$ are decoupled and are solved by Maliuzhinets [14]:

$$\bar{G}_z(\alpha)=\begin{bmatrix}\Psi_e(\alpha) & 0\\ 0 & \Psi_h(\alpha)\end{bmatrix}\begin{bmatrix}a^0_1\\ a^0_2\end{bmatrix}, \tag{9}$$

where $a^0_1$ and $a^0_2$ are arbitrary constants, and

$$\begin{aligned}\Psi_{e,h}(\alpha)=&\,\psi\big(\alpha+v^{e,h}_1\big)\psi\big(\alpha+\pi-v^{e,h}_1\big)\\&\times\psi\big(\alpha+v^{e,h}_2-\pi\big)\psi\big(\alpha-v^{e,h}_2\big).\end{aligned} \tag{10}$$

The Maliuzhinets function $\psi(\alpha)$ of wedge with angle $\pi$ is defined as

$$\psi(\alpha)=\exp\left(\frac{1}{4\pi}\int_0^\alpha\frac{2u-\pi\sin u}{\cos u}du\right). \tag{11}$$

The asymptotic behavior of $\psi(\alpha)$ is

$$\lim_{|\mathrm{Im}(\alpha)|\to\infty}\psi(\alpha)=O\left[\exp\left(\frac{|\mathrm{Im}(\alpha)|}{4}\right)\right]. \tag{12}$$

Combining Eqs. (9) and (7), we can get the expression for the spectral function $\bar{F}_z(\alpha)$.

It was first discovered by Vaccaro that if $\bar{G}_z(\alpha)$ in Eq. (9) is the solution to Eq. (8), $\bar{G}_z(\alpha)\sigma(\alpha)$ where $\sigma(\alpha)$ satisfies $\sigma(\alpha\pm\frac{\pi}{2})=\sigma(-\alpha\pm\frac{\pi}{2})$ will also be the solution [12]. It is easy to show that $\sin^n(\alpha)$, where $n$ is an integer is a solution of $\sigma(\alpha)$. Hence, Eq. (9) can be generalized as [18]

$$\begin{aligned}\bar{G}_z(\alpha)=&\begin{bmatrix}\Psi_e(\alpha) & 0\\ 0 & \Psi_h(\alpha)\end{bmatrix}\Bigg(\begin{bmatrix}a^{-1}_1\\ a^{-1}_2\end{bmatrix}\frac{1}{\sin\alpha-\cos\phi'}\\&+\begin{bmatrix}a^0_1\\ a^0_2\end{bmatrix}+\begin{bmatrix}a^1_1\\ a^1_2\end{bmatrix}\sin\alpha+\cdots\Bigg),\end{aligned} \tag{13}$$

where $\phi'$ is the incident angle as shown in Fig. 1(a) and $a^n_{1,2}$ are constants we need to figure out. From Eqs. (12) and (10), we know that $\lim_{|\mathrm{Im}(\alpha)|\to\infty}\Psi_{e,h}(\alpha)=O(\exp(|\mathrm{Im}(\alpha)|))$ and $\lim_{|\mathrm{Im}(\alpha)|\to\infty}\bar{\bar{C}}^{-1}(\alpha-\frac{\pi}{2})=O(\exp(-|\mathrm{Im}(\alpha)|))$. Combining that with Eq. (3), we can conclude that $a^n_{1,2}=0$ for $n\geqslant 1$. The first-order pole caused by $a^{-1}_{1,2}$ is produced by the incident wave in the driven mode. For the eigenmode case, we can set

$a_{1,2}^{-1} = 0$ directly. The spectral function $\bar{F}_z(\alpha)$ can be expressed as

$$\bar{F}_z(\alpha) = \bar{\bar{C}}^{-1}\left(\alpha - \frac{\pi}{2}\right)\begin{bmatrix}\Psi_e(\alpha) & 0\\ 0 & \Psi_h(\alpha)\end{bmatrix}\begin{bmatrix}a_1^0\\ a_2^0\end{bmatrix} \tag{14}$$

$a_{1,2}^0$ and eigenvalue $\beta$ are calculated by removing the poles introduced by $\bar{\bar{C}}^{-1}(\alpha - \frac{\pi}{2})$, which have no physical interpretation. The poles $\alpha_0^{\pm}$ can be defined as

$$\cos\left(\alpha_0^{\pm} - \frac{\pi}{2}\right) \mp i \sin\left(\alpha_0^{\pm} - \frac{\pi}{2}\right)\cos\beta = 0. \tag{15}$$

The process of removing the poles $\alpha_0^{\pm}$ is to find appropriate eigenvalue $\beta$ and eigenvector $a_{1,2}^0$ that satisfied the equations $\bar{F}_z(\alpha_0^{\pm})[\cos^2(\alpha_0^{\pm} - \frac{\pi}{2}) + \sin^2(\alpha_0^{\pm} - \frac{\pi}{2})\cos^2\beta] = 0$. It can be further expressed as

$$\begin{bmatrix} i\Psi_e(\alpha_0^+) & \Psi_h(\alpha_0^+)\\ -i\Psi_e(\alpha_0^-) & \Psi_h(\alpha_0^-)\end{bmatrix}\begin{bmatrix}a_1^0\\ a_2^0\end{bmatrix} = 0. \tag{16}$$

In order to have nonzero solution of $a_{1,2}^0$, it requires

$$\det\left(\begin{bmatrix} i\Psi_e(\alpha_0^+) & \Psi_h(\alpha_0^+)\\ -i\Psi_e(\alpha_0^-) & \Psi_h(\alpha_0^-)\end{bmatrix}\right) = 0. \tag{17}$$

Keep in mind that $\Psi_{e,h}(\alpha_0^{\pm})$ as defined by Eq. (10) are functions of $\beta$. By solving Eq. (17), we can get the eigenvalue $\beta$. It is shown in Ref. [9] that the energy of the electromagnetic wave is confined near $\rho = 0$ and decays exponentially as $\rho$ grows. Hence, it is intuitive to predict that the eigenvalue $\beta$ should satisfy $|\cos\beta| > 1$, which means $|k_z| > k_0$. Plugging $\beta$ into Eq. (16), we can solve $a_{1,2}^0$ and finally get the spectral function $\bar{F}_z(\alpha)$.

Once the spectral function $\bar{F}_z(\alpha)$ is achieved, we can figure out $E_z$ and $H_z$ in real space by applying Eq. (2). The integral path as shown in Fig. 2 is symmetric to the origin in the $\alpha$ plane [20]. The ends of $\gamma_{\pm}$ are located in those regions where $\mathrm{Re}(-ik_0\rho\sin\beta\cos\alpha) < 0$ so that the factor $e^{-ik_0\rho\sin\beta\cos\alpha}$ decays as $|\mathrm{Im}(\alpha)| \to \infty$. Since $|\cos\beta| > 1$ and the impedance

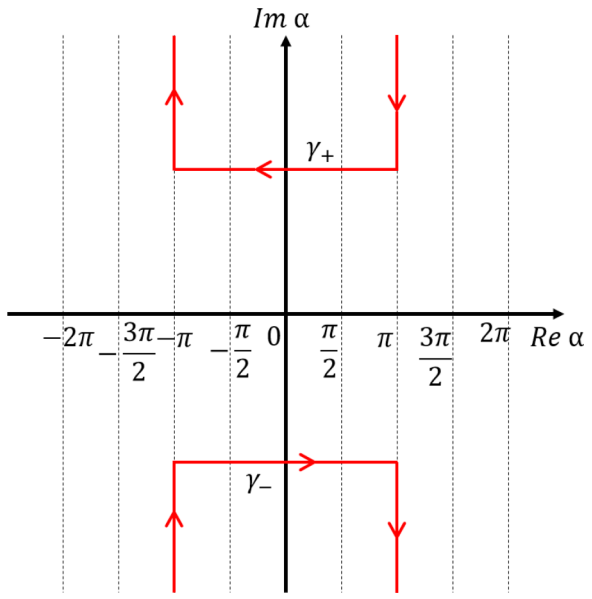


FIG. 2. Integration path $\gamma$.

surface is lossless, we know that $\sin\beta$ is purely imaginary. Without loss of generality, we assume $\mathrm{Im}(\sin\beta) > 0$. To ensure the fastest decay of $e^{-ik_0\rho\sin\beta\cos\alpha}$, it is assumed that the ends of $\gamma_+$ are located at $\pi + i\infty$ and $-\pi + i\infty$ and the ends of $\gamma_-$ are at $-\pi - i\infty$ and $\pi - i\infty$. Although the poles introduced by $\bar{\bar{C}}^{-1}(\alpha - \frac{\pi}{2})$ which have no physical interpretation have been removed, the poles introduced by $\Psi_{e,h}(\alpha)$ still exist. The poles of the Maliuzhinets function $\psi(\alpha)$ are all on the real axis of the $\alpha$ plane. According to the definition of $\Psi_{e,h}(\alpha)$ given in Eq. (10), the poles are shifted to the region with $\mathrm{Im}(\alpha) \neq 0$ due to the fact that $\mathrm{Im}(v_{1,2}^{e,h})$ may be nonzero. In order to ensure that no singularities of the integrand function are located in the regions bounded by $\gamma_{\pm}$ above $\gamma_+$ and below $\gamma_-$, the integral path should be chosen sufficiently far from the real axis. For simplicity, we choose $\gamma_+ = (i\infty + \pi, id + \pi] \cup [id + \pi, id - \pi] \cup [id - \pi, i\infty - \pi)$, where $d$ can be any constant that satisfies $d > |\mathrm{Im}(v_{1,2}^{e,h})|$.

## III. NUMERICAL RESULTS AND DISCUSSION

Numerical results will be presented in the section to verify the accuracy of proposed analytical representation. The two-dimensional (2D) model in COMSOL is chosen for comparison since we neglect the $z$ dependence of field, which is in the form of $e^{ik_0 z\cos\beta}$ when showing the result.

### A. Eigenvalue verification

Since we assume the surface impedance $Z_1$ and $Z_2$ are constants and the structure is invariant under the scaling transform, $k_z/k_0$ should be a constant that will not vary with $k_0$, which means $\cos\beta$ should be a constant only related to $Z_1$ and $Z_2$. The method to figure out $\cos\beta$ is to solve Eq. (17). By sweeping the value of $\cos\beta$, we can easily find the correct solution as shown in Fig. 3. Comparing with the result simulated by COMSOL, we find the high accuracy of our method when calculating the eigenvalue $\cos\beta$. Here the surface impedances $Z_1$ and $Z_2$ are inductive and capacitive impedance respectively. When they are both inductive or capacitive, no eigenmode will exist. Because of the inversion symmetry in the $z$ axis, if $\cos\beta$ is one solution for the eigenvalue, then $-\cos\beta$ will also be a solution. For simplicity, we only focus on the positive $\cos\beta$. As shown in Fig. 3, $|\cos\beta| > 1$ is satisfied for different values of $Z_1$ and $Z_2$, which indicates the energy of the electromagnetic field is confined near the interface between the two surfaces. Also, larger values of $|\cos\beta|$ represent better confinement of the eigenfield. Hence, the case when $Z_1 = -iZ_0/\sqrt{3}$, $Z_2 = \sqrt{3}iZ_0$ in Fig. 3(a) decays faster in the $\rho$ direction than the case when $Z_1 = -iZ_0/2$, $Z_2 = 2\sqrt{2}iZ_0$ in Fig. 3(c).

### B. Eigenfield verification

When Eq. (17) is satisfied, Eq. (16) will have a nonzero solution for $\begin{bmatrix}a_1^0\\ a_2^0\end{bmatrix}$. We will take $\begin{bmatrix}\Psi_h(\alpha_0^+)\\ -i\Psi_e(\alpha_0^+)\end{bmatrix}$ in the following derivation. Assuming the case when $Z_1 = -i/2\sqrt{2}Z_0$ and $Z_2 = 2iZ_0$, we can achieve the eigenvalue $\cos\beta = 1.7205$ by sweeping the parameter as mentioned. Also, we can get $a_1^0 = -0.1143 + 0.3244i$ and $a_2^0 = 0.1359 - 0.3858i$. By inserting the values of $a_1^0$ and $a_2^0$ into Eq. (14), we have

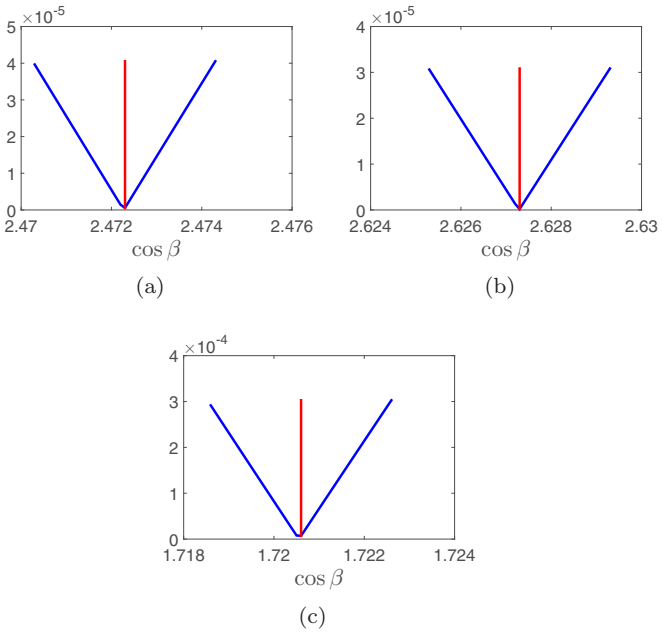


FIG. 3. Absolute value of the determinant defined in Eq. (17) when sweeping $\cos\beta$ (blue line) and eigenvalue $\cos\beta$ calculated by COMSOL (red line) for (a) $Z_1 = -iZ_0/\sqrt{3}$, $Z_2 = \sqrt{3}iZ_0$; (b) $Z_1 = -iZ_0/\sqrt{2}$, $Z_2 = 2iZ_0$; and (c) $Z_1 = -iZ_0/2$, $Z_2 = 2\sqrt{2}iZ_0$.

completely solved the spectral function $\bar{F}_z(\alpha)$. One last step is to define the integration path $\gamma$ in order to calculate $E_z$ and $H_z$ in real space as shown in Eq. (2). We choose $\gamma_+ = (i\infty + \pi,\ id + \pi] \cup [id + \pi,\ id - \pi] \cup [id - \pi,\ i\infty - \pi)$ where $d$ satisfies the condition $d > |\mathrm{Im}(v_{1,2}^{e,h})|$. Here we have $v_1^e = \pi/2 - 1.3286i$, $v_1^h = -0.2553$, $v_2^e = -0.3652$, $v_2^h = \pi/2 - 0.8955i$. We set $d = \pi$ and the integration path becomes $\gamma_+ = (i\infty + \pi, i\pi + \pi] \cup [i\pi + \pi, i\pi - \pi] \cup [i\pi - \pi, i\infty - \pi)$, $\gamma_- = (-i\infty - \pi, -i\pi - \pi] \cup [-i\pi - \pi, -i\pi + \pi] \cup [-i\pi + \pi, -i\infty + \pi)$.

As shown in Fig. 4, we set $\phi = \pi/3$ as a constant and sweep the value of $k_0\rho$ from 0.1 to 1.0. Both $E_z$ and $Z_0H_z$ are normalized by $E_z(k_0\rho = 0.1)$ so we can compare the analytic solution with the COMSOL simulation result. Figure 4(a) shows that both $|E_z|$ and $|H_z|$ decrease with the increase of $k_0\rho$ and the analytic solution matches well with the simulation result.

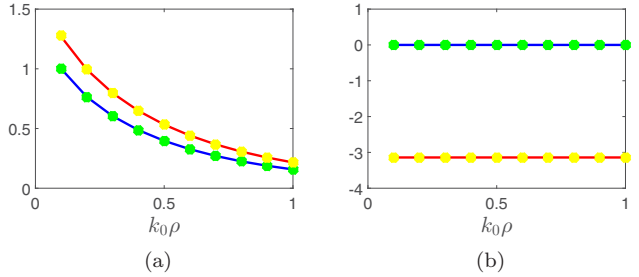


FIG. 4. (a) Absolute value and (b) phase of normalized electric field $E_z/E_z(k_0\rho = 0.1)$ (blue line for analytic solution and green dots for COMSOL simulation) and normalized magnetic field $Z_0H_z/E_z(k_0\rho = 0.1)$ (red line for analytic solution and yellow dots for COMSOL simulation), when $\phi = \pi/3$.

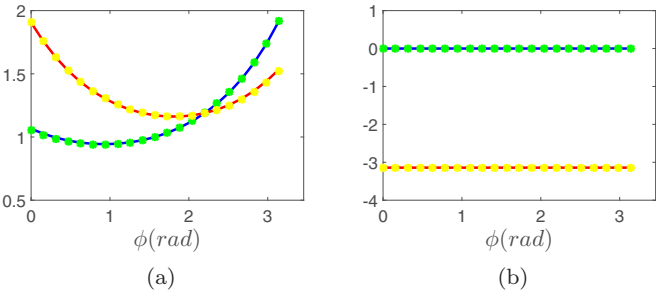


FIG. 5. (a) Absolute value and (b) phase of normalized electric field $E_z/E_z(\phi = \pi/2)$ (blue line for analytic solution and green dots for COMSOL simulation) and normalized magnetic field $Z_0H_z/E_z(\phi = \pi/2)$ (red line for analytic solution and yellow dots for COMSOL simulation) when $k_0\rho = 0.5$.

The phase of the eigenfield along the $\rho$ axis is a constant which can be concluded from Fig. 4(b).

Similar to Fig. 4, we set $k_0\rho = 0.5$ as a constant and sweep $\phi$ from 0 to $\pi$ in Fig. 5. Divided by $E_z(\phi = \pi/2)$, the normalized eigenfield calculated by the analytic method shows high accuracy. From Fig. 5(a), we can conclude that the absolute value of $E_z$ and $H_z$ will not vary monotonically with the increase of $\phi$, but instead they increase after reaching a minimum at a particular value of $\phi$. Figure 5(b) shows that the phase is also a constant when $k_0\rho$ is fixed. Combined with result in Fig. 4(b), we predict that both $E_z$ and $H_z$ have same phase throughout the $xy$ plane.

The absolute values of the normalized electric field $|E_z/E_z(k_0\rho = 0)|$ and normalized magnetic field $|H_zZ_0/E_z(k_0\rho = 0)|$ are plotted in Figs. 6 and 7 respectively. The phases are neglected here since we can conclude from Figs. 4(b) and 5(b) that the phases of $E_z$ and $H_z$ are uniformly distributed in the $xy$ plane. As we can see, the field is concentrated at the interface between two complementary surfaces where $\rho = 0$ and decays exponentially as $\rho$ grows. Both $E_z$ and $H_z$ are finite at $\rho = 0$, which satisfies the boundary condition while $E_\rho$, $E_\phi$, $H_\rho$, and $H_\phi$ can have a singularity at the edge [9,19]. The field is not symmetrically distributed about axis $\phi = \pi/2$ since for $E_z$ the left part $\pi/2 < \phi < \pi$ is larger while for $H_z$ the right part $0 < \phi < \pi/2$ is larger. It is more clear in Fig. 8, where the ratio of electric field and magnetic field $|E_z/(H_zZ_0)|$ is plotted. The value will increase as $\phi$ varies from 0 to $\pi$ for a constant $\rho$.

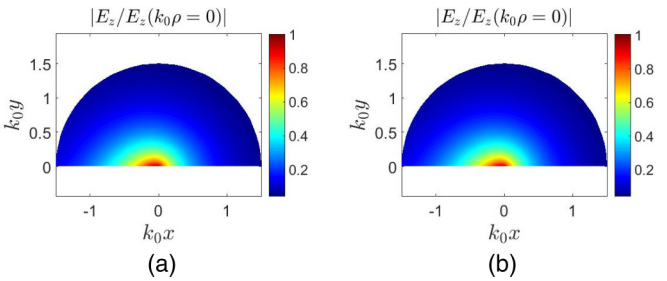


FIG. 6. Normalized electric field $|E_z/E_z(k_0\rho = 0)|$ calculated by (a) analytic method and (b) COMSOL simulation.

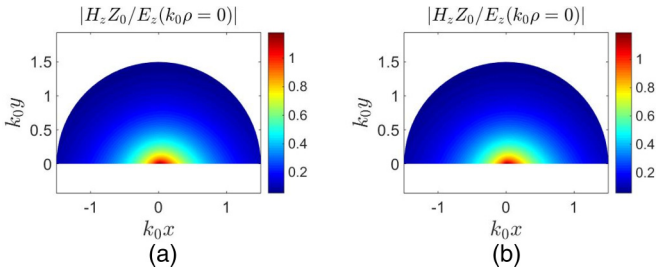


FIG. 7. Normalized magnetic field $|H_zZ_0/E_z(k_0\rho = 0)|$ calculated by (a) analytic method and (b) COMSOL simulation.

Once we figure out the value of $E_z$ and $H_z$, it is easy to get the value of transverse electric field $E_\rho$, $E_\phi$ by applying (similarly for transverse magnetic field)

$$E_\rho = \frac{i}{k_0 \sin^2\beta}\left(\cos\beta\frac{\partial E_z}{\partial\rho} + \frac{1}{\rho}\frac{\partial Z_0H_z}{\partial\phi}\right), \tag{18a}$$

$$E_\phi = \frac{i}{k_0 \sin^2\beta}\left(\cos\beta\frac{1}{\rho}\frac{\partial E_z}{\partial\phi} - \frac{\partial Z_0H_z}{\partial\rho}\right). \tag{18b}$$

Alternatively, we can also solve them by the Sommerfeld-Maliuzhinets technique and the derivative in Eq. (18) turns into multiplication in the spectral domain through $\partial/\partial\rho \to -ik_0\sin\beta\cos\alpha$, $\partial/\partial\phi \to ik_0\rho\sin\beta\sin\alpha$. Equation (18) can be rewritten as

$$E_\rho = \frac{e^{ik_0z\cos\beta}}{2\pi i\sin\beta}\int_\gamma [\cos\beta\cos\alpha, -\sin\alpha]\bar{F}_z\left(\alpha+\frac{\pi}{2}-\phi\right) \times e^{-ik_0\rho\sin\beta\cos\alpha}d\alpha, \tag{19a}$$

$$E_\phi = -\frac{e^{ik_0z\cos\beta}}{2\pi i\sin\beta}\int_\gamma [\cos\beta\sin\alpha, \cos\alpha]\bar{F}_z\left(\alpha+\frac{\pi}{2}-\phi\right) \times e^{-ik_0\rho\sin\beta\cos\alpha}d\alpha. \tag{19b}$$

The spectral functions of $E_\rho$ ($[\cos\beta\cos\alpha, -\sin\alpha]\bar{F}_z/\sin\beta$) and $E_\phi$ ($-[\cos\beta\sin\alpha, \cos\alpha]\bar{F}_z/\sin\beta$) tend to infinity when $|\mathrm{Im}(\alpha)| \to \infty$, which indicates $E_\rho$ and $E_\phi$ will tend to infinity at $\rho \to 0$ in real space. However, the volume integrals of $|E_\rho|^2$ and $|E_\phi|^2$ are still finite for finite volume around $\rho = 0$ since the energy should be finite for any practical physical system. As shown in Fig. 9, the transverse electric field decays when $\rho$ increases, which also matches the simulation results in Ref. [9].

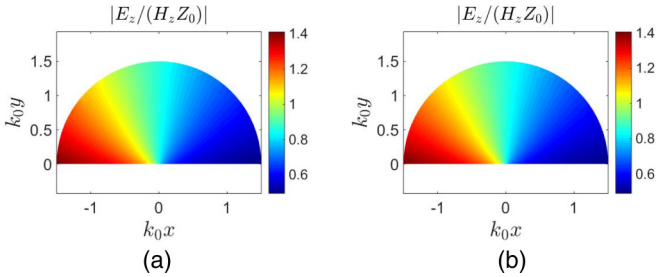


FIG. 8. $|E_z/(H_zZ_0)|$ calculated by (a) analytic method and (b) COMSOL simulation.

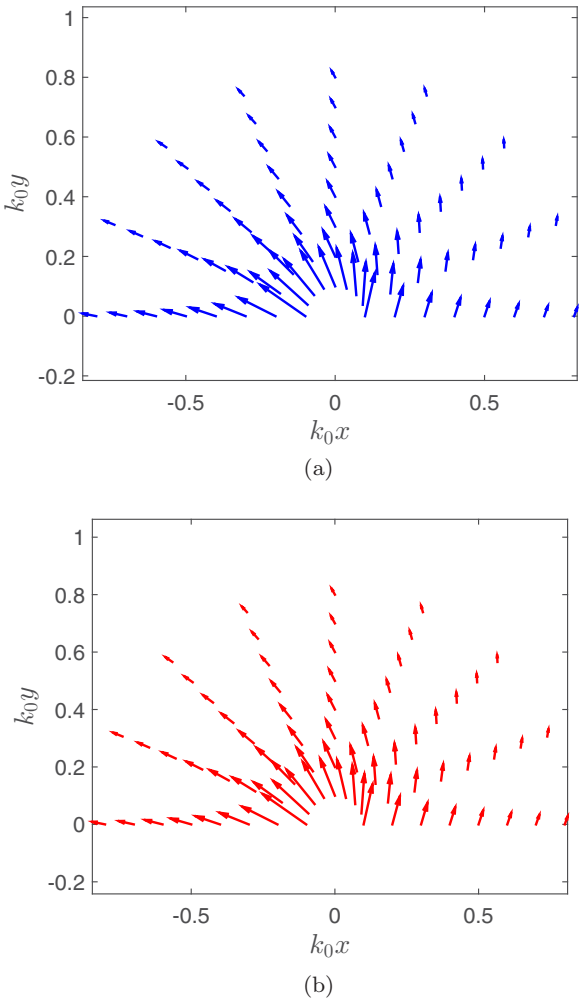


FIG. 9. Real part of the transverse electric field calculated by (a) applying Eq. (19) and (b) COMSOL simulation is plotted.

### C. Characteristic impedance and phase velocity of the waveguide

The phase velocity of the structure shown in Fig. 1(b) can be calculated by

$$v_p = \frac{\omega}{k_z} = \frac{c}{\cos\beta}, \tag{20}$$

where $c$ is the speed of light in vacuum and $\cos\beta$ is the eigenvalue mentioned above.

Also, we can follow the definition given in Ref. [21] and define the characteristic impedance as

$$Z_c = \frac{2P}{I^2}, \tag{21}$$

where

$$P = \frac{1}{2}\mathrm{Re}\left[\iint (E_t \times H_t^*)_z dxdy\right] \tag{22}$$

and

$$I = \int_{-\infty}^{+\infty} J_z dx = \int_{-\infty}^{+\infty} -H_x dx. \tag{23}$$

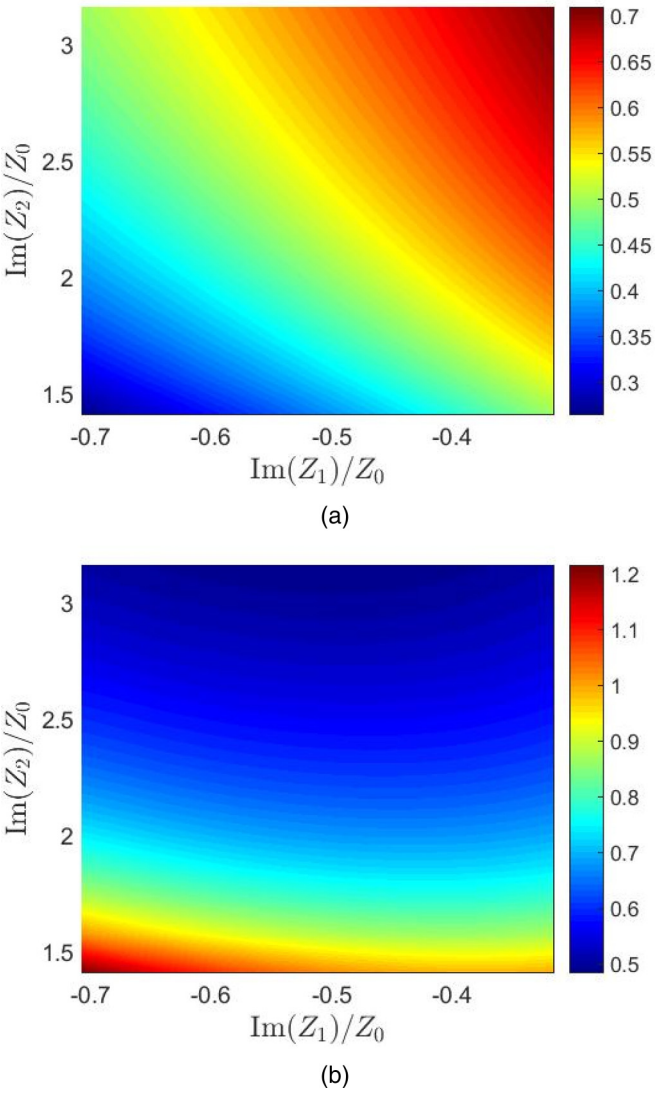


FIG. 10. (a) Normalized phase velocity $v_p/c$ and (b) normalized characteristic impedance $Z_c/Z_0$ are plotted as functions of $Z_1$ and $Z_2$.

The integrand in Eq. (22) is the $z$ component of the Poynting vector and the integral domain is the cross section above the impedance surface. $J_z$ in Eq. (23) is the current density on the surface, which has the same value as $-H_x$ on the impedance surface.

As shown in Fig. 10, since we assume the complementary impedance surfaces are lossless, both $Z_1$ and $Z_2$ are purely imaginary with opposite sign. With the increase of $\mathrm{Im}(Z_1)$ and $\mathrm{Im}(Z_2)$, the phase velocity will increase monotonically, which means the energy will be less confined near $\rho = 0$ according to the definition in Eq. (20). Besides, the phase velocities have an upper bound since they cannot exceed the speed of light, which is also shown in Fig. 10(a). Similarly, we can achieve larger characteristic impedance for smaller $\mathrm{Im}(Z_1)$ and $\mathrm{Im}(Z_2)$ as shown in Fig. 10(b).

## IV. CONCLUSIONS

An analytic solution of the eigenmode of a wedge structure with two complementary surface impedances has been carried out by using the generalized reflection method which is developed from the Sommerfeld-Maliuzhinets technique. Compared with the driven mode which can also be solved by generalized reflection method, both spectral function $\bar{F}_z(\alpha)$ and integration path $\gamma$ have to be modified in order to make the method effective. The analytic theory not only proves the existence of an edge mode but also provides the theoretical support for understanding the relation between edge modes and diffraction from a wedge structure. The results are useful because we have also calculated the waveguide properties such as characteristic impedance and phase velocity for the structure.

## ACKNOWLEDGMENTS

This work was supported in part by Air Force Office of Scientific Research Grant No. FA9550-16-1-0093 and in part by the China Scholarship Council (No. 201706230113).

[1] B. A. Bernevig, T. L. Hughes, and S.-C. Zhang, Science **314**, 1757 (2006).
[2] C. L. Kane and E. J. Mele, Phys. Rev. Lett. **95**, 146802 (2005).
[3] A. B. Khanikaev, S. H. Mousavi, W.-K. Tse, M. Kargarian, A. H. MacDonald, and G. Shvets, Nat. Mater. **12**, 233 (2013).
[4] T. Ma, A. B. Khanikaev, S. H. Mousavi, and G. Shvets, Phys. Rev. Lett. **114**, 127401 (2015).
[5] L. Lu, J. D. Joannopoulos, and M. Soljačić, Nat. Photon. **8**, 821 (2014).
[6] S. Raghu and F. D. M. Haldane, Phys. Rev. A **78**, 033834 (2008).
[7] C. He, X. Ni, H. Ge, X.-C. Sun, Y.-B. Chen, M.-H. Lu, X.-P. Liu, and Y.-F. Chen, Nat. Phys. **12**, 1124 (2016).
[8] R. Süsstrunk and S. D. Huber, Proc. Natl. Acad. Sci. USA **113**, E4767 (2016).
[9] J. B. Dia'aaldin and D. F. Sievenpiper, Phys. Rev. Lett. **119**, 106802 (2017).
[10] D. J. Bisharat and D. F. Sievenpiper, Nanophotonics **7**, 893 (2018).
[11] D. R. Mason, S. G. Menabde, S. Yu, and N. Park, Sci. Rep. **4**, 4536 (2014).
[12] V. Vaccaro, AEU-Archiv Electronik Ubertragungstechnik—Int. J. Electronics Commun. **34**, 493 (1980).
[13] V. G. Vaccaro, Optica Acta: Int. J. Optics **28**, 293 (1981).
[14] G. D. Maliuzhinets, Soviet Phys. Doklady **3**, 752 (1958).
[15] J. Bernard, J. Phys. A: Math. Gen. **31**, 595 (1998).

[16] A. Vallecchi, Electromagnetics **33**, 73 (2013).
[17] M. A. Lyalinov and N. Y. Zhu, IEEE Trans. Antennas Propag. **61**, 329 (2013).
[18] R. G. Rojas, IEEE Trans. Antennas Propag. **36**, 956 (1988).
[19] J. Meixner, IEEE Trans. Antennas Propag. **20**, 442 (1972).
[20] A. V. Osipov and S. A. Tretyakov, *Modern Electromagnetic Scattering Theory with Applications* (John Wiley & Sons, New York, 2017).
[21] W. Marynowski, P. Kowalczyk, and J. Mazur, Prog. Electromagn. Res. **110**, 219 (2010).